Cyclic Voltammetry Studies of Nanoporous Semiconductors. Capacitive and Reactive Properties of Nanocrystalline TiO_2 Electrodes in Aqueous Electrolyte

Francisco Fabregat-Santiago,* Ivan Mora-Seró, Germà Garcia-Belmonte, and Juan Bisquert*

Departament de Ciències Experimentals, Universitat Jaume I, 12080 Castelló, Spain

Received: July 13, 2002; In Final Form: October 16, 2002

Extended networks of nanosized semiconductor particles permeated with an electrolyte display unique electrochemical behaviors. We report on a general investigation of the electrochemical properties of nanoporous electrodes by means of cyclic voltammetry. Models have been developed accounting for the fundamental characteristics of these electrodes: charge accumulation, charge transport, and interfacial charge transfer. These characteristics can be translated into simple electrical equivalents, which allow us to identify and classify the major features of voltammetry response according to the competition of the different processes during a voltammetric scan. A key point for describing the experimental observations is the potential dependence of the intrinsic film capacitance. The physical meaning of this capacitance is discussed in terms of the distribution of electronic states. We describe in detail the numerical simulation methods, and despite the simplicity of our approach, we show that these methods allow for quantitative description of experimental data of nanoporous TiO_2 electrodes in aqueous electrolyte, including the determination of the density of states and the absolute energy levels.

1. Introduction

Nanoscaled materials have become very important for recent technological developments in broad fields: photovoltaics, photocatalysis, energy storage (batteries, supercapacitors), sensing, medicine and biophysics, catalysis, etc. Nanostructured electrode materials may belong, for example, to the groups of porous semiconductors, organic nanocomposites, or sintered nanoporous metal oxides. In this paper, we investigate the electrochemical properties of nanostructured electrodes by means of cyclic voltammetry. As a prototype of nanoscaled electrodes with a varying electron density, we take the nanoparticulate semiconductor networks, composed of small and low-doped metal-oxide crystallites (in the 10 nm range) sintered in a connected structure on top of a conducting substrate or, in brief, nanoporous semiconductor electrodes. This is a promising class of electrode materials (including TiO_2 and ZnO) for technical applications such as dye sensitized solar cells and photocatalysis.

In a certain sense nanoporous electrodes belong to the wider class of porous electrodes, which have been widely investigated in electrochemistry. Recently, Conway and co-workers have discussed the main features of cyclic voltammograms (CVs) of polarizable porous electrodes in relation with supercapacitor applications.[1−3] These authors have shown that a simple and satisfactory description of CVs of porous electrodes can be made combining two types of elements: a capacitance related to double-layer or redox process or both and a series resistance linked to transport of the charged species. Here, we adopt a similar approach, but to extend the analysis of Conway et al. to other classes of systems, including metal-oxide semiconductor nanoporous electrodes, we must take into account the general features of new nanoporous systems as described in the following.

A crucial characteristic of nanoporous semiconductor electrodes permeated with a conductive phase is the ability to accumulate a large number of injected electron charges in the solid matrix.[4] We will generally assume that nanoparticles contain a very low density of dopant, although the specific case of highly doped nanoparticles will be treated separately below. Then, a combination of several factors (the small size of basic constituents, a good electronic connectivity between nanosized elements, and the presence of a surrounding equipotential surface) permits us to control in a simple way the electron Fermi level, E_{Fn}, in the semiconductor network. The displacement of the Fermi level toward the semiconductor conduction band produces a homogeneous increase of the electron concentration in the film. This property can be characterized by an intrinsic differential capacitance that increases hugely with the potential.[5−7] A similar feature can be found in other types of electroactive films, such as ion insertion materials,[8] redox and electronically conducting polymers,[9,10] and supercapacitors,[1] all of which show a large capacitance associated with charging a solid matrix. In some of these systems, anodic and cathodic CV peaks are basically related to the exhaustion of available sites for the injected or adsorbed species (redox capacitance or pseudocapacitance).[1,9] However, the interpretation of major CV peaks observed in nanoporous semiconductor electrodes requires a specific description of the electronic states in this system that will be discussed in section 3.

While the intrinsic capacitance should be a permanent feature in semiconductor nanoporous electrodes, their electrochemical behavior is significantly influenced by the rate of charge transfer, which depends on the presence of redox species in the solution and on the overlap of the electronic levels in the semiconductor surface with those in the redox couple.[11] Therefore, it is also necessary to consider faradaic (resistive) components related to charge transfer at the internal semiconductor/electrolyte interface. In addition, a series resistance represents the combina-

* To whom correspondence should be addressed. E-mail addresses: bisquert@uji.es, fabresan@uji.es.

10.1021/jp0265182 CCC: $25.00
Published on Web 11/15/2002

tion of bulk electrolyte, resistivities at substrate and wire contacts, and intrinsic transport components related both to the porous network and electrolyte in the voids.

By combining these elements, we introduce here a new model with simple features as a powerful tool for describing the experimental data. Although CVs of nanoporous semiconductor electrodes have been reported many times,[12−19] to our knowledge a complete analysis considering these features has not been reported so far. Here, a combined study of experimental CVs and electrochemical impedance of TiO_2 nanoporous electrodes shows that the new model is suitable for quantitative description of the major features observed in the CVs and for extracting additional information on the properties of these electrodes.

In the next section, we describe the results of the measurements. Section 3 gives an overview of the features of the capacitance in a nanoporous system, an outline of the models for CVs and the simulations, and in section 4, we present the discussion. We finish with conclusions in section 5.

2. Experimental Results on Nanoporous TiO_2 Films

2.1. Materials and Apparatus. Electrochemical measurements were done in a standard three-electrode cell using a Ag/AgCl (in aqueous KCl 3 M) reference electrode and a Pt counter electrode. With the aim of studying the effect of the series resistance on voltammetry results, aqueous electrolyte solutions were adjusted to different pHs, 2, 3, 4, and 11, with H_2SO_4 to obtain the acidic ones and KOH to obtain the basic ones. This changed the contribution of the solution, and accordingly the series resistance measured was 30, 82, 262, and 181 Ω, respectively.

CVs and impedance spectra were obtained with an Autolab PGSTAT-30 equipped with a frequency analyzer module. The samples used in this work were two films of nanoporous anatase TiO_2 made from the deposition of 23.3 nm average diameter colloids on a fluorine-doped tin oxide (FTO) transparent conducting substrate with a film thickness of 2.6 μm and surfaces of 2.7 and 2.9 cm^2, denoted as samples A and B, respectively.

2.2. Cyclic Voltammetry Results. A selection of the typical patterns of CVs that were found at all of the pHs for the two samples measured is presented in Figures 1−3. Figure 1 presents the effect of changing the return voltage at pH 2 and fixed scan rate $s = 50$ mV s^{-1}. Figure 2 shows the effect of the variation of the scan rate at pH 3, and Figure 3 shows the CV at pH 11 and $s = 100$ mV s^{-1}. Figure 4 shows the variation of peak current with respect to change of both scan rate and series resistance (by varying the pH in the electrolyte as indicated above).

In Figure 1, the cathodic current follows an exponentially rising behavior in all cases. A clear anodic peak is observed after the return voltage has been reached; however, prior to this point, a cathodic peak is never obtained even though the return potentials move progressively further in the negative direction. These common features observed for all of the CVs of Figure 1 present a characteristic difference (apart from the charge involved in the polarization process), which is specially visible at the two extreme returning potentials measured: At the most negative, Figure 1a, the return current line presents a certain inclination until it achieves the anodic peak, while at the less cathodic return voltage, Figure 1b, this line is vertical.

By changing the scan rate, Figure 2, it is found that the shape at the highest speeds is the same as that in the previous case (Figure 1). But at a lower speed, 5 mV s^{-1}, the features are distinctly different. Instead of an exponential variation, the

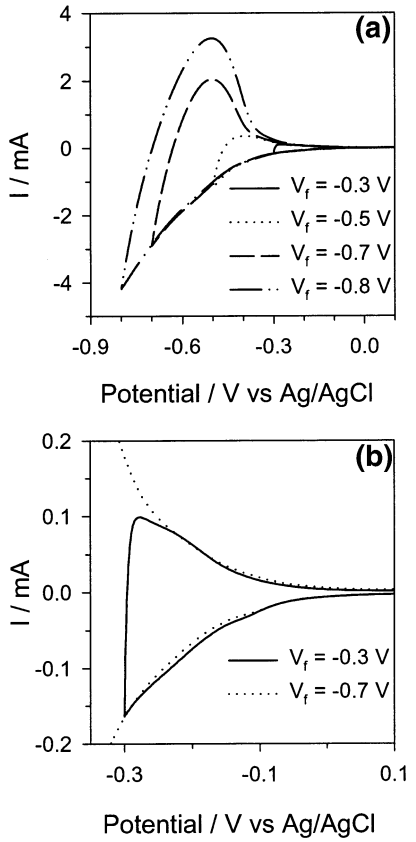

Figure 1. Experimental series (a) of voltammetries made over sample A at pH 2 and a constant scan rate of 50 mV s^{-1} with different return potentials as indicated and (b) a zoom of panel a showing the voltammetries with return potentials of −0.3 and −0.7 V.

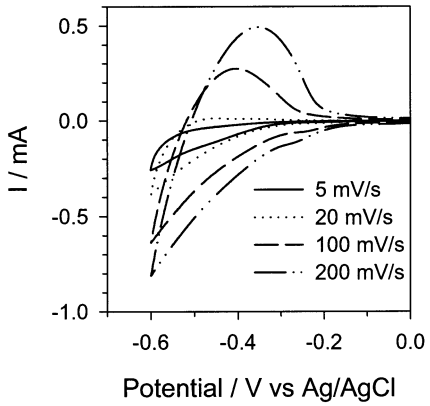

Figure 2. Experimental series of voltammetries made over sample A in pH 3 aqueous solution taken at different scan rates as indicated.

cathodic current exhibits an approximately linear growth, and beyond the return potential, the voltammogram shows a more or less wide pattern, but current reversal and formation of an anodic peak are not obtained in this case. As is well-known, this behavior indicates that current losses dominate, although charge is accumulated in the film to a certain extent. An extreme case of this type of situation can be seen in Figure 3, in which the CV presents an almost ideal faradaic behavior with negligible accumulation.

The small local peak that may be observed at low potential in Figure 2 is generally attributed to intraband gap localized states.[15,20−23] The charging of deep surface states levels, and subsequent charge transfer causes important effects for many applications, but for simplicity, we defer the detailed analysis of these effects to a future work.

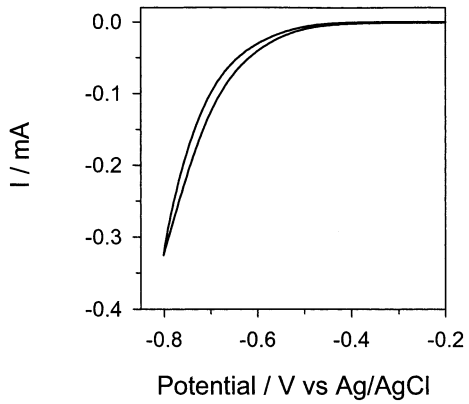

Figure 3. Experimental voltammetry of sample B made in a pH 11 aqueous solution at a scan rate of 100 mV s^{-1}.

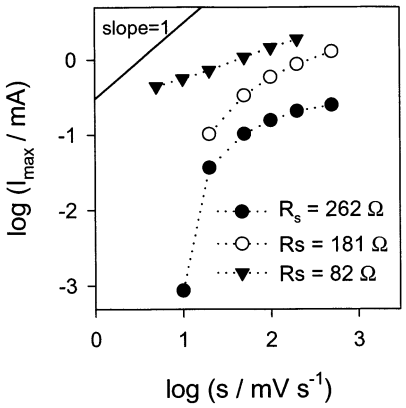

Figure 4. Experimental peak currents vs scan rate of the voltammetries taken over sample A at pH 3 (R_s = 82 Ω), pH 11 (R_s = 181 Ω), and pH 4 (R_s = 262 Ω).

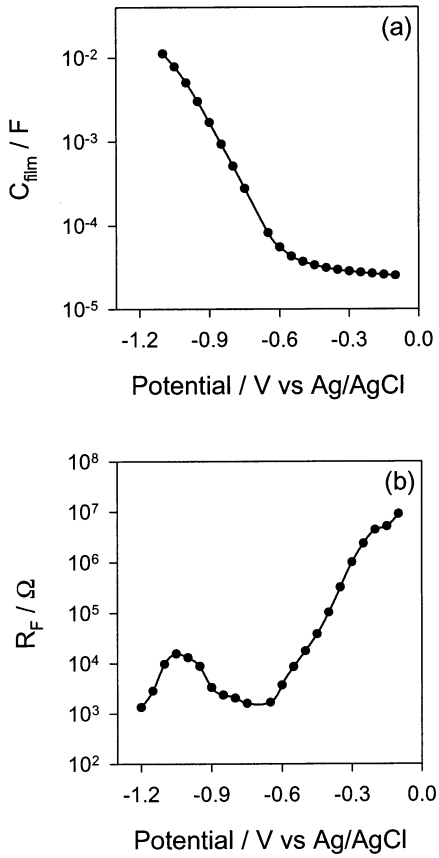

Figure 5. Experimental film capacitance (a) and faradaic charge-transfer resistance (b) determined by impedance spectroscopy of sample B at pH 11.

It is seen in Figure 2 that at increasing speeds, both the total charge involved in the polarization process and the reversibility of the cycle increase, indicating a larger domination of charge accumulation mechanisms. It is well-known that the peak current should increase linearly with the scan rate if a capacitive behavior prevails. Figure 4 shows that at the highest values of *s* the slope tends to a constant value in a double logarithmic plot, but actually it never reaches the theoretical value 1. Furthermore, the slope changes with the pH, and in some cases, at low *s* the points deviate strongly from a straight line.

The origin of these characteristic shapes of CV and this last result will be described in the next sections.

2.3. Impedance Results. The electrochemical impedance technique operates by a small modulated perturbation over a steady state, and therefore, it supplies a general view of the main capacitive and resistive processes and their dependence on the steady-state potential. To acquire complementary information on the different processes contributing to the observed CV currents, we studied the electrochemical impedance spectra of the films in the range of potentials in which the CVs were measured, and we applied the methods of interpretation of impedance that have been amply described in a previous work.[4]

The impedance results obtained, shown in Figure 5 (for pH 11), were very similar to those previously reported[4] and may be resumed in two main regions. The first one, at very low cathodic potentials, is dominated by a low capacitance, which follows a Mott−Schottky behavior, Figure 5a, which is attributed to FTO substrate/electrolyte interface.[4,24]

At higher cathodic potentials, there occurs a faradaic loss of charge through the film that is accounted for a faradaic resistance, R_F, placed in parallel with the capacitor. R_F shows an exponential decay with the applied potential, Figure 5b, with slope varying between 125 and 250 mV/decade, depending on potential range and pH. At a certain voltage, R_F rises in the cathodic direction indicating that saturation of faradaic current is reached as found in planar TiO_2 electrodes.[25] Finally, at the highest negative applied potentials, R_F decays again and tends to stabilize. At a certain potential in this highly cathodic region, the capacitance changes from a Mott−Schottky behavior to an exponential increase with the cathodic potential, which shows pH-dependent slopes between 180 and 240 mV/decade, Figure 5a, the onset of which has been found to be also dependent on pH. In the impedance results for the more acidic electrolyte solutions (not shown), the potential of the characteristic capacity onset and the faradaic resistance saturation exhibit a displacement toward anodic values, and greater values of the intrinsic film capacitance are found.

As shown in the previous paper,[4] there is a potential region that departs from this simple model because diffusion processes become significant in a narrow range (150 mV wide) at very low cathodic voltages. The application of a diffusion impedance model permits us to determine the electron conductivity while it is relatively low.[4] However, in the case of CVs, the major features occur at high currents in states of a large electronic conductivity, so diffusion has been neglected in this work.

3. Model

As commented in the Introduction, a major feature of low-doped nanoporous semiconductor electrodes is that they can acquire voltage-injected electrons by a wide displacement of the Fermi level with respect to the edge of the conduction band.

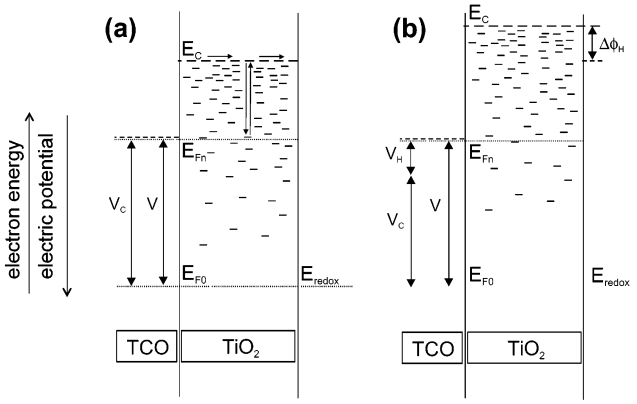

Figure 6. Scheme of electronic states in a TiO_2 nanoporous electrode permeated with a redox electrolyte. In panel a, the scheme shows two classes of electronic states in the TiO_2: extended states (conduction band) of energy E_c and an exponential distribution of band gap localized states. The extended electronic states serve as a relay to communicate all of the band gap states with the transparent conducting oxide (TCO) by a process of trapping and release. Therefore, the Fermi level E_{Fn} is controlled by the potential V in the TCO and determines the occupancy of both the extended and localized states. In panel b, under partial band unpinning by charging at the Helmholtz layer, the cell potential is $V = V_C + V_H$, where $V_H = \Delta\phi_H$ and V_C indicates the true displacement of E_{Fn} with respect to E_c.

When the resistive effects can be neglected (e.g., the electrode operates in an inert solution and transport losses have been minimized), the CV is described by a capacitance related to the occupancy of electronic states in the network.[5−7] In the following, we begin with the capacitance model for CVs, and subsequently, we outline increasingly more general models, adding up progressively the transport series resistance and the faradaic parallel resistance related to charge transfer at the oxide/solution interface. Numerical simulations of the different models are presented in Figures 7−9.

3.1. Intrinsic Capacitance of Film Electrodes. As mentioned, we assume now that the rate of electron transfer between nanoparticles and solution is negligible; interfacial charge-transfer effects will be considered later on. In such conditions, the electrode response is that of a capacitance $C = dQ/dV$, and the CV current is

$$I = \frac{dQ}{dt} = Cs \tag{1}$$

where $s = dV/dt$ is the scan rate. Therefore the CVs will be completely described if the film capacity, related to electron accumulation in the nanoparticles, is known as a function of the electrode potential. Because this capacity is a crucial feature for a suitable description of CVs, we provide in the following a discussion of this concept.

In Figure 6, we present a plausible distribution of electronic states in the TiO_2 nanoparticles consisting of two classes of states: One is a band of extended states at energy E_c with density N_c and the other one a wide distribution of monoelectronic band gap localized states. The occupancy of these states is determined by the electrode potential, V. This potential is defined as the difference of Fermi levels of the macroscopic metal contacts (electron reservoirs), that is, the conducting substrate of the nanoporous working electrode (in the left) and the counter electrode (in the right), $V = -(E_{Fn} - E_{redox})/e$. We will assume that the Fermi level in the counter electrode is pinned to the redox potential of the solution, E_{redox}. When the working electrode is unbiased, the Fermi level is homogeneous in the cell, so $E_{F0} = E_{redox}$. When the left electrode is biased negatively and we wait for equilibrium to be reached in the film, we obtain a homogeneous upward shift of the Fermi level in the whole semiconductor network, $dE_{Fn} = -e\,dV$, implying a change of occupancy of the electron states. Let us assume for the moment that the energy level E_c is stationary as indicated in Figure 6a (i.e., band edge pinning conditions; the more general case without this restriction will be discussed later on). We consider one specific state like those shown in Figure 6, characterized by the energy E. This energy is defined to be increasingly negative for states deeper in the gap. The average occupancy is described by the Fermi−Dirac distribution function

$$f(E - E_{Fn}) = \frac{1}{1 + \exp[(E - E_{Fn})/(k_B T)]} \tag{2}$$

A displacement of the Fermi level causes a variation of the state occupancy in the following way:

$$\frac{df}{dE_{Fn}} = \frac{1}{k_B T} f(1 - f) \tag{3}$$

The capacitance is defined as the variation of electrical charge of the single state associated with the change dV of the electrical potential. Therefore, we have, for a single electronic state,

$$C = -e\frac{df}{dV} = e^2\frac{df}{dE_{Fn}} = \frac{e^2}{k_B T} f(1 - f) \tag{4}$$

To obtain the electrode capacitance per substrate area related to charging this type of state, we simply multiply eq 4 by LN, where L is the film thickness and N is the volume concentration of the state. To obtain the total film capacitance, we multiply eq 4 by the density of states function and integrate over all energies, see below.

We remark that eq 4 implies that $C(V)$ peaks at the energy of the electronic state, E, with a peak width of $\sim 2k_BT$, provided that the Fermi level passes across the state through $f = 1/2$. This explains the small local CV peak related to a monoenergetic band gap state commented in the preceding section.[15] The capacitance peak related to exhaustion of an energy level is also the main feature of a redox capacitance as defined for electronic and redox polymers.[9,26] The situation is somewhat different in the presence of a wide distribution of energies, Figure 6, as discussed in the following.

The occupancy of extended states at E_c is normally well-described by the Boltzmann limit, that is, $E_c - E_{Fn} \gg k_BT$ implying $f \ll 1$, and the free electron density may be written $n = N_c f = N_c\, e^{(E_{Fn} - E_c)/(k_B T)}$. Hence, the conduction band capacitance is given by the following equivalent expressions

$$C_{cb} = -LN_c\frac{e^2}{k_B T} f = L\frac{e^2 n}{k_B T} = L\frac{e^2}{k_B T} n_0\, e^{(E_{Fn} - E_c)/(k_B T)} \tag{5}$$

where n_0 is the concentration at zero bias. If we define $C_{cb0} = Le^2 n_0/(k_B T)$ and the homogeneous film potential $V_C = -(E_{Fn} - E_{F0})/e$, we can write

$$C_{cb} = C_{cb0}\exp[-eV_C/(k_B T)] \tag{6}$$

Therefore, the capacitance of conduction band states increases exponentially with the bias voltage.

Next, we consider the distribution of band gap states, $g(E)$ (per unit volume and eV), as shown in Figure 6. Integrating all of the contributions, eq 4, through the band gap, we obtain

$$C = Le^2 \int_{-\infty}^{+\infty} g(E) \frac{df}{dE_{Fn}} dE \quad (7)$$

Using $df(E - E_{Fn})/dE_{Fn} = -df(E - E_{Fn})/dE$ and integrating eq 7 by parts, we arrive at

$$C = Le^2 \int_{-\infty}^{+\infty} \frac{dg}{dE} f(E - E_{Fn}) dE \quad (8)$$

A simple solution to eq 8 is obtained by the zero temperature limit of the Fermi function, that is, a step function at $E = E_{Fn}$ separating occupied from unoccupied states. Then, it follows that

$$C = Le^2 \int_{-\infty}^{E_{Fn}} \frac{dg}{dE} dE = Le^2 g(E_{Fn}) \quad (9)$$

In this approximation, eq 9, the charging related to the perturbation dV corresponds to filling a slice of traps at the Fermi level. A similar idea is expressed in refs 23 and 27.

As a particularly important distribution of traps, we consider the exponential band tail of states in the gap

$$g(E) = \frac{\Theta_t}{k_B T_c} \exp[(E - E_c)/(k_B T_c)] \quad (10)$$

where Θ_t represents the total volume density of traps and the parameter T_c is a characteristic temperature that defines the tail shape (broadening) of the exponential distribution. The distribution can be characterized also by the coefficient $\alpha_c = T/T_c$, which takes typical values near $\alpha_c = 0.5$ ($k_B T_c = 50$ meV).[28−31] The capacitance, in the approximation of eq 9, takes the form

$$C_{trap} = L\frac{\alpha_c e^2 \Theta_t}{k_B T} e^{-\alpha_c (E_c - E_{Fn})/(k_B T)} = L\frac{\alpha_c e^2 \Theta_t}{k_B T N_c^{\alpha_c}} n^{\alpha_c} \quad (11)$$

(In ref 7, another prefactor appears in eq 11 because eq 8 was solved considering also the thermally occupied states between E_{Fn} and E_c.) Hence, the trap capacitance depends on the voltage as

$$C_{trap} = C_{trap0} \exp[-\alpha_c e V_C/(k_B T)] \quad (12)$$

In eq 12, we obtain as in eq 6 an exponential dependence of $C(V)$. In eq 6, the capacitance corresponds to the Boltzmann tail of the electron distribution, so the reason for not obtaining a peak is that the Fermi level does not cross the conduction band edge. In eq 12, the exponential dependence is a direct translation of the density of states at the Fermi level. It must be noted that eq 12 provides a variation with voltage that is much slower than the Boltzmann factor ($\alpha_c < 1$ at room temperature).

We have remarked that the porous semiconductor network is characterized by a homogeneous Fermi level determined by the substrate potential. Let us examine the necessary conditions for this state of affairs. When the substrate is biased, initially a gradient of the Fermi level will exist, which will drive electron to the low E_{Fn} regions until equilibrium is reached. In the model schematized in Figure 6a, the electron transport occurs through a band of extended states at energy E_c. Thereafter, the localized band gap states attain the equilibrium occupancy imposed by the substrate potential by a process of trapping and detrapping of electrons at E_c. Finally, all of the electronic states in the porous network satisfy the Fermi−Dirac distribution with a common Fermi level. We note that the presence of extended states is not a necessary requirement for achieving the equilibrium distribution. (In fact, in our measurement, C_{cb} has not been observed, as discussed below.) This can be obtained also by other transport mechanisms: trapping and detrapping from localized transport states at E_c with density $N_c = g(E_c)$, hopping between traps, provided that the density is large enough for the quantum-mechanical tunneling transitions from one trap to another to occur at a sufficiently fast rate, and electronic transitions from one particle to another. Independent of the actual conduction mechanism that predominates in a given situation, a certain degree of electronic conductivity is required for achieving a homogeneous charging in the film. Therefore, we expect that under a scan of the stationary potential at progressively more cathodic values, the exponential voltage-dependent capacitance will have an onset at a certain potential. When E_{Fn} is deep in the gap so that conductivity of the semiconductor network is poor, biasing the electrode produces a certain electrical potential distribution near the substrate[32,33] and the electron accumulation process responds to other factors, such as the substrate/electrolyte interface, as mentioned before. After the onset of conductivity, the equilibration process will be fast and the charging will be described by the homogeneous capacitance of eq 4. This general behavior is in agreement with the observations presented in Figure 5.

The concept of a intrinsic film capacity that we have discussed so far has been introduced recently in the area of nanoporous electrodes.[5−7] In essence, this type of capacitance is given by the reciprocal of the derivative of the *chemical potential* function with respect to concentration. The concept is known since much earlier in other areas. An equilibrium differential capacitance is defined for ion intercalation films[8] in the lattice gas model approach to the chemical potential of intercalated ions and reproduces eq 4 in the absence of interactions. This idea was exported later on to the fields of redox polymers and electronically conducting polymers in which it is known as a redox capacity.[9] A similar concept can be derived from the Langmuir adsorption isotherm (pseudocapacitance).[26] Independently, an equivalent idea was extensively used in the theories for hopping conductivity in disordered semiconductors (see, for example, ref 34). In this last field, the capacitance associated with each localized electronic state is defined with respect to the local electrochemical potential, as we have done above, eq 4.

An equivalent approach leading to the intrinsic film capacitance starts from an electron diffusion model. Because diffusion is driven by a gradient of the chemical potential, at very low frequencies the impedance of diffusion provides the capacitance of eq 6; thus, the conventional diffusion capacitance of semiconductor device theory[35] is a concept similar to the intrinsic film capacitance of nanoporous electrodes. However, it is important to realize that the capacity defined above is determined by the equilibrium properties, so the presence of diffusion is not a necessary requirement to define these capacitances. This was not clearly recognized in semiconductor physics because it is normally not possible to vary the Fermi level in a homogeneous way in solid-state devices. By contrast, this is very easy in the nanoporous devices, as already discussed, so the film capacitance of eq 9 measures directly the density of states function. A general analysis of thermodynamics functions and diffusion impedance in electroactive materials has been presented in recent works.[36,37]

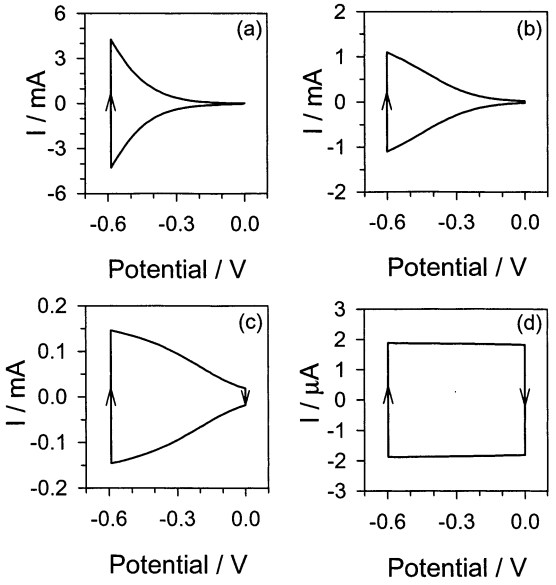

Figure 7. Simulation of cyclic voltammograms between $V_1 = 0$ V and $V_2 = -0.6$ V for an exponential capacitance with a series Helmholtz capacitance. In all cases, $s = 200$ mV s^{-1}, $\alpha = 0.25$ (exponential slope of 240 mV per decade), $C_a = 0.1$ mF, and $R_s = 30\ \Omega$. The different panels correspond to (a) $C_H = 100$ mF, (b) $C_H = 10$ mF, (c) $C_H = 1$ mF, and (d) $C_H = 0.01$ mF.

The two capacitances defined in eqs 6 and 12 respond to the same potential, V_C, and are therefore connected in parallel. We will assume that one of them predominates, and taking into account the observed, quasi-constant capacitance at low potentials (C_b), we will use in the model for CV the general form

$$C = C_a \exp[-\alpha e V_C/(k_B T)] + C_b \tag{13}$$

where C_a is the prefactor of the exponential increase and $\alpha \leq 1$ is now a coefficient describing either the Boltzmann occupancy of the conduction band capacitance ($\alpha = 1$) or an exponential distribution of trap states ($\alpha = \alpha_c < 1$). In our measurements, α took values between 0.33 and 0.25, therefore meaning that the injected electrons are predominantly stored in band gap states in an exponential distribution with these values of α_c. We remark that our measurements do not show an indication of the charging of conduction band states (C_{cb} varying at 59 mV/decade), although this could be explained if $C_{cb} \ll C_{trap}$.

The CV shape associated with eq 13 (with $C_b = 0$) is illustrated in Figure 7a. It is seen that the CV during each scan direction reflects directly the shape of the capacitance as a function of voltage, eq 1, and the line shape is symmetric because of sign reversal of s.

3.2. Band Unpinning and Highly Doped Nanoparticles. So far it has been assumed that the energies of the various electronic states are stationary against a variation of the electrode potential, that is, band pinning conditions. However, for maintaining charge neutrality into the electrode, it is required that the increasing electron charge in the particles be accompanied by positive ion charge at the semiconductor/electrolyte interface. As is well-known and shown in Figure 6b, surface charging changes the potential difference in the Helmholtz layer, producing an upward shift of the semiconductor energy levels, $V_H = \Delta\phi_H$. An analysis presented elsewhere[7] shows that the combined effect of electron accumulation and partial band unpinning can be accounted for by a constant Helmholtz capacitance, C_H (per unit macroscopic area), connected in series to the intrinsic film capacitance, C_i, so the electrode capacitance becomes

$$C = (C_i(V_C)^{-1} + C_H^{-1})^{-1} \tag{14}$$

In principle, the CV can be characterized using eqs 1 and 14; however, to apply eq 14, it is necessary to determine the relationship of V_C to the cell potential, V, during a scan at a constant rate. If the bias voltage, $V = -(E_{Fn} - E_{F0})/e$, causes a shift of the conduction band from E_{c0} to E_c (Figure 6), the potential V_C in eq 14 refers to the actual displacement of E_{Fn} relative to E_c. Therefore, we must write, generalizing the definition given above eq 6,[7]

$$V_C = -(E_{Fn} - E_{F0})/e + (E_c - E_{c0})/e \tag{15}$$

hence, the cell potential can be expressed (see Figure 6b)

$$V = V_C + V_H \tag{16}$$

By continuity of current, one has

$$I = C_i \frac{dV_C}{dt} = C_H \frac{dV_H}{dt} \tag{17}$$

From $s = dV/dt$, using eqs 16 and 17, we obtained that

$$s = \left(1 + \frac{C_i(V_C)}{C_H}\right) \frac{dV_C}{dt} \tag{18}$$

For a constant s and substituting eq 13 for $C_i(V_C)$, we can readily integrate eq 18, giving an analytical formula $t(V_C)$, which enables us to calculate the current with eq 17. This procedure is applied to calculate the line shape of CVs in Figure 7 at varying values of C_H. Obviously, the significance of band unpinning increases as C_i becomes equal to or larger than C_H, as illustrated in Figure 7. In an intermediate situation in which both capacitances reach a similar size, the increasing $\Delta\phi_H$ produces a progressive flattening of the original exponential CV, as shown in Figure 7b,c. If C_i becomes significantly larger than C_H at all of the potentials, then the film is in the state of Fermi level pinning, the capacitance is a constant, and so is the CV current, as illustrated in Figure 7d.

In our measurements, we are in the case in which the capacity of the film is still much lower than the Helmholtz capacity (except when the electrode potential is very close to E_c; see section 4). This may be checked by comparing Figures 1, 2, and 7 or, alternatively, contrasting the values of the capacitance presented in Figure 5 with data reported previously.[38,39] Therefore in a first approximation, the potential drop at the Helmholtz layer will be neglected hereafter.

We have so far discussed the capacitive properties of low-doped nanoporous semiconductor electrodes. The picture is essentially different for *heavily doped* nanoparticles, which can be formed, for example, from SnO_2.[40,41] Here, in the bulk of the particles, the electron concentration is fixed and there is no possible displacement of E_{Fn} with respect to E_c. When the left electrode is biased negatively both E_{Fn} and E_c move together, that is, the potential changes at the Helmholtz layer at the particle's surface, so the CV will tend to a flat characteristic, as already discussed and observed for porous silicon.[42] In addition, each nanoparticle contains a space-charge depletion layer at the surface. Therefore, if a n-type material electrode is biased positively, the surface band bending will increase, providing a Mott−Schottky characteristic in the capacitance−voltage dependence.[40,41] In this case, it is possible to define a

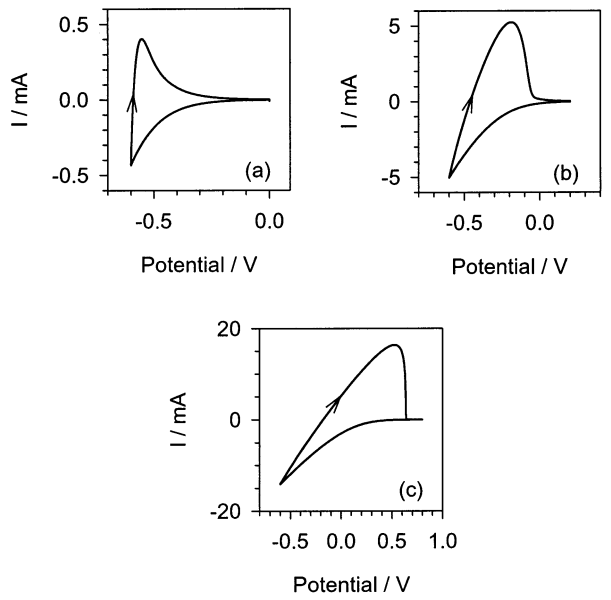

Figure 8. Simulation of cyclic voltammograms for an exponential capacitance with a series resistance R_s. $V_2 = -0.6$ V, $s = 100$ mV s^{-1}, $\alpha = 0.25$, and $R_s = 30\ \Omega$ are kept constant, while C_a and V_1 take the values (a) $V_1 = 0$ V, $C_a = 10^{-5}$ F, (b) $V_1 = 0.2$ V, $C_a = 10^{-3}$ F, and (c) $V_1 = 0.8$ V, $C_a = 10^{-1}$ F.

flatband potential for the nanoporous semiconductor in the conventional way.

3.3. Effect of the Series Resistance. The transport of electronic and ionic species is associated with gradients of the respective electrochemical potentials, which take a fraction of the potential difference in the external circuit; therefore, we must write the cell potential as $V = V_C + V_T$, where V_T is associated with the transport components. To treat such feature in a simple way, we consider a model that contains, in addition to the film capacitance, a constant series resistance R_s related to transport, so that when the CV current is I, we have $V_T = IR_s$. This is a suitable description of transport in the bulk electrolyte outside the film. However, an accurate treatment in the electroactive film necessitates an advanced transport model, considering position-dependent concentrations of ionic and electronic species, and a consistent extension of the film capacitance and faradaic resistance to account for the local degree of electron accumulation and charge-transfer rate. Here, we restrict ourselves to a homogeneous model introduced in the previous subsections, aiming to investigate the major features of CVs by the competition of the different effects. This approach is justified provided that gradients of carriers and concentration inhomogeneity consist of second-order corrections with respect to the huge exponential variation of the main electrode characteristics. Theoretical confirmation of this point is left as a matter for future investigations. For the moment, the support of the present approach rests in the agreement with the observation.

In the following, we discuss intuitively the general features of the R_sC model. Thereafter, we present the simulation equations and results in Figure 8 and a general discussion of the possible CV behaviors in this model. The additional effect of a faradaic resistance will be considered in the next subsection.

Let us start with the main effect of the series resistance on the purely exponential capacitive shape described in Figure 7a. In Figure 1, it is observed that the symmetric shape obtained under completely capacitive charging (at $V_2 = -0.3$ V) is progressively distorted along the x axis as the return voltage becomes more negative. Such distortion can be understood by the presence of a series resistance. Distortion owing to this factor increases at more negative voltage because the current grows rapidly, and consequently, the fraction of the voltage absorbed by the series resistor increases, that is, $V = V_C + IR_s$. We remark on the interpretation of the applied potential in the context of this model. The only point at which the applied voltage coincides with the capacitor potential, $V = V_C$, is that at which $I = 0$. Moreover, this specific value of potential is the most negative value reached by V_C. In fact, the potential V_C increases up to this value while the current is *negative*. The fact that the cell potential V surpasses this value in the negative direction corresponds to partial potential drop in the series resistance, $V_T = IR_s$. It follows that, assuming that faradaic losses can be neglected, even if the CVs are distorted in this way it is possible to determine readily the relationship $Q(V_C)$ (and then the film capacitance by $C = dQ/dV$) by stepping the CVs at progressively more negative return potentials. Then $Q(V_C)$ results from integrating in each case the negative current in two steps: as it increases and then as it decreases or otherwise, equivalently, integrating the discharging, positive current.

We now develop the equations that determine the CV current in the R_sC model. As already pointed out, the presence of a series resistance R_s implies that the capacitance potential V_C (the local electrode potential following the nomenclature of Pell and Conway[2]) is not equal to the cell potential. In a CV experiment, while polarizing in the cathodic direction between the cell potential limits of V_1 and V_2, V_C is

$$V_C = V_1 - st - R_sI_c \tag{19}$$

In the same way, during the anodic polarization between the cell potential limits of V_2 and V_1, V_C is

$$V_C = V_2 + st - R_sI_a \tag{20}$$

On the other hand, the intensity of current that passes through the cell may be described by

$$I = \frac{dQ}{dt} = \frac{dQ}{dV_C}\frac{dV_C}{dt} = C\frac{dV_C}{dt} \tag{21}$$

In our case C is described by eq 13, which combined with eqs 19, 20, and 21 allows us to obtain the differential equations that describe $V_C(t)$. Therefore, for an exponential capacitance with a series resistance, we have

$$\frac{dV_C}{du} = \{\exp[-\alpha eV_C/(k_BT)] + C_b/C_a\}^{-1}(V_1 - \omega u - V_C) \tag{22}$$

for the cathodic direction and

$$\frac{dV_C}{du} = \{\exp[-\alpha eV_C/(k_BT)] + C_b/C_a\}^{-1}(V_2 + \omega u - V_C) \tag{23}$$

for the anodic direction, where $u = t/\tau$, $\tau = R_sC_a$, and $\omega = s\tau$.

Equations 22 and 23 have been solved numerically, by the method of Runge−Kutta of fourth order, starting from $V_C(t=0) = 0$ V and using parameters based on those obtained by impedance. Once $V_C(t)$ was known, the intensity of current, I, could be easily determined by means of eqs 19 and 20, and finally, we could represent the results as in standard CV experiment, I vs V_{cell}, Figure 8.

In this figure, all of the possible different patterns of a CV of the RC circuit are shown, just varying the preexponential parameter C_a. The distortion introduced by the series resistance

over the CV shape of the bare capacitance of Figure 7a increases as C_a (or ω) is raised; therefore, Figure 8a (C_a low) presents a close resemblance to Figure 7a, which disappears at higher values of C_a, Figure 8b. When C_a (or ω) is large, the behavior of the cathodic current departs from the exponential, tending to a linear increase with a slope of $1/R_s$, Figure 8c. This is because the high value of C_a involves a low V_C potential, which becomes insignificant with respect to R_sI in eqs 19 and 20. Therefore, one can regard this change of shape as the transition from a capacitive to a resistive regime.

As already noted, in the series R_sC system, the capacitor stores charge during the cathodic direction of the voltammogram and during the anodic direction while the current is negative. When the current on anodic direction becomes positive, the capacitor returns all of the charge accumulated giving rise to a peak with a certain I_{max} value at positive current, as illustrated in Figure 7 and further discussed below. It must be recognized that the return peaks illustrated in Figure 8 are not related to a diffusion-limited redox process, but instead correspond to the same exponential capacitive process as that of Figure 7a.

We have investigated the effects of variations of different parameters and combinations of them on simulated CVs. For a constant value of the return potential, V_2, the shape and the scale do not change if ω and R_s are kept constant. Modifications of just this last parameter introduce only variations of scale due to the presence of R_s in the calculation of the current in eqs 19 and 20. Changes in V_2 tune the pattern and scale of CVs in a similar way as those in ω and R_s, but an exact correlation could not be found.

In summary, for a short scan range voltammogram, the current is very low and the term R_sI of eqs 19 and 20 can be neglected with respect to V_C, giving a nearly capacitance pattern. On the other hand, as V_2 is shifted in the cathodic direction, the current increases exponentially and the term R_sI takes relevance until it prevails at negative enough return potential, changing the CV to the resistive regime with a linear shape. In all of these cases, a large positive peak is observed corresponding to discharge of the charge accumulated in the capacitor while the current was negative.

3.4. Effect of Parallel Charge-Transfer Resistance. The presence of nonnegligible charge transfer from the nanoporous semiconductor to the surrounding electrolyte alters fundamentally the previous picture, because now there are two components to current, that of charging the capacitor and that of electrons jumping to electrolyte acceptor levels.

In principle, as the electron density increases in the semiconductor, the charge-transfer resistance, R_F, should decrease in an exponential fashion with increasingly cathodic potential. If the exchange of electrons between the semiconductor and redox species in solution occurs via surface states, the behavior of R_F is more complex.[11] Such behavior appears to occur in the measurements reported in Figure 5b and will be treated in more detail elsewhere. To handle the behavior of R_F in a simple way, it was modeled as an exponential function of V_C, which levels off to a constant value at very negative potentials:

$$R_F = R_{Fa} \exp[\alpha_t e V_C/(k_B T)] + R_{Fb} \quad (24)$$

where α_t is the transfer coefficient of the faradaic reaction, R_{Fa} is the prefactor of the exponential, and R_{Fb} is the lower charge-transfer limit taken in our simplification.

If the charge-transfer process as described by eq 24 dominates the current in the CV, then the current at any time is a unique function of voltage, independent of scan direction, so the values of I coincide in the cathodic and anodic scans, which is nearly the case in Figure 3.

We now consider the general situation extending the model of subsection 3.3 to take into account the faradaic resistance, which is connected in parallel to the exponential capacitance. In this case, the eqs 19 and 20 remain unchanged but, as already mentioned, now there are two contributions to the total current, the current flow through R_F, I_F, and the charging current through C, I_C:

$$I = I_C + I_F \quad (25)$$

Because C and R_F are connected in parallel, we have

$$I_C = C \frac{dV_C}{dt} \quad (26)$$

$$I_F = V_C/R_F \quad (27)$$

Combining the eqs 13, 19, 20, and 24−27, we obtain the differential equations that describe this case for the cathodic direction

$$\frac{dV_C}{du} = \frac{1}{A(V_C)}\left\{V_1 - \omega u - V_C\left(1 + \frac{R_s}{R_{Fa}}\frac{1}{B(V_C)}\right)\right\} \quad (28)$$

and for the anodic direction

$$\frac{dV_C}{du} = \frac{1}{A(V_C)}\left\{V_2 + \omega u - V_C\left(1 + \frac{R_s}{R_{Fa}}\frac{1}{B(V_C)}\right)\right\} \quad (29)$$

where we write $A(V_C) = C_b/C_a + \exp[-\alpha e V_C/(k_B T)]$ and $B(V_C) = R_{Fb}/R_{Fa} + \exp[\alpha_t e V_C/(k_B T)]$ to simplify these equations.

In the same way that the presence of a series resistance R_s modifies the voltammogram pattern of a capacitance, as discussed formerly, now the presence of a parallel charge-transfer resistance R_F modifies the patterns obtained in the previous subsection. Figure 9a shows the different behaviors of the voltammogram as R_{Fa} varies. When R_{Fa} is very large, I_F is low and the current is dominated by I_C, so the CV pattern is close to that obtained for the case with only an exponential capacitance with a series resistance. On the other hand, when R_{Fa} decreases, the faradaic current through R_F increases, eventually becoming prevalent.

If we consider again the case in which the charge-transfer current can be neglected ($R_{Fa} \rightarrow \infty$), we recall that the CV shows always a large peak in the positive current region as shown in Figure 8. By contrast, when the faradaic current dominates, the current through the capacitor is low and the charge accumulated becomes insignificant, so the peak in positive current constitutes a minor feature or even disappears completely, as can be observed in Figure 9a for the case with $R_{Fa} = 10^4\ \Omega$. When R_F becomes very low (case $R_{Fa} = 10^3\ \Omega$ in Figure 9a), the observed current is independent of scan direction.

Figure 9b presents the different behaviors obtained when s is varied at fixed $R_{Fa} = 10^5\ \Omega$. We can observe that the faradaic current increases as s decreases. This fact is due to the linear decrease of I_C with s, eq 21.

3.5. Behavior of the Peak Current, I_{max}, with Respect to Scan Rate, s. The models developed allow the study of the relation between I_{max} and s. In the case with only one capacitance, there exists a linear dependence of I_{max} on s, eq 21, which, represented in a double logarithmic scale, has a slope of 1. As is well-known, this slope will be modified if a series resistance is introduced. Figure 10a shows the behavior

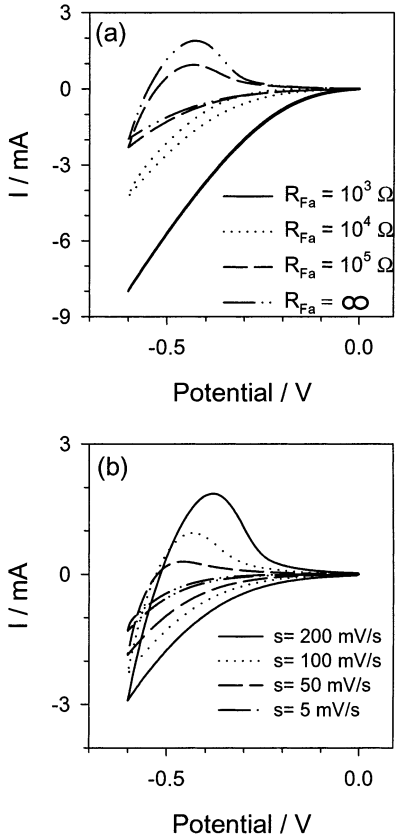

Figure 9. Simulation of cyclic voltammograms for an exponential capacitance in parallel with an exponential charge-transfer resistance plus a series resistance R_s. $V_1 = 0$ V, $V_2 = -0.6$ V, $s = 100$ mV s^{-1}, $\alpha = \alpha_t = 0.25$, $C_a = 10^{-4}$ F, and $R_s = 30\ \Omega$ are kept constant. Panel a presents a comparative graphic that shows the different simulations obtained when varying R_{Fa}, as indicated. Panel b presents a comparative graphic that shows the different behaviors obtained for $R_{Fa} = 10^5\ \Omega$ when varying s, as indicated.

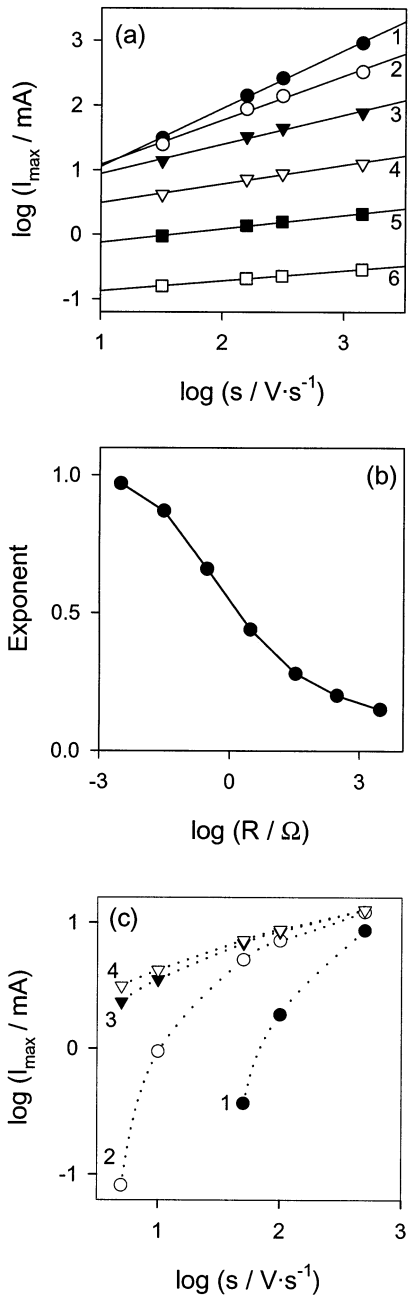

Figure 10. Simulation of the variation of peak current with scan rate. Panel a shows log(I_{max}) as function of log(s) for an exponential capacitance with different series resistances R_s. $V_1 = 0$ V, $V_2 = -1$ V, $s = 100$ mV s^{-1}, $\alpha = 0.25$, and $C_a = 10^{-4}$ F are kept constant, while R_s takes the values (1) 0.003, (2) 0.03, (3) 0.3, (4) 3, (5) 30, and (6) 300 Ω. Panel b shows exponent values of $I_{max} = As^b$ as function of R_s, obtained from the linear fit of the data shown in panel a. Panel c shows log(I_{max}) as a function of log(s) for the exponential capacitance of eq 13 in parallel with the exponential charge-transfer resistance, R_F, of eq 24, plus a series resistance with changing R_{Fa} values. $V_1 = 0$ V, $V_2 = -1$ V, $s = 100$ mV s^{-1}, $\alpha = \alpha_t = 0.25$, $C_a = 10^{-4}$ F, and $R_s = 30\ \Omega$ are kept constant, while $R_{Fa} =$ (1) 10^5, (2) 10^6, (3) $10^7\ \Omega$, and (4) ∞.

of log(I_{max}) vs log(s), for the simulation of the exponential capacitance with the series resistance for different R_s values. The nearly linear shape of these plots implies a dependence $I_{max} = As^b$ in the range of scan rates used. The exponents corresponding to best fits are presented in Figure 10b, which shows that the exponent tends to 1 as R_s decreases. Variation of return potential in the cathodic direction has the opposite effect on this slope as CV turns into a resistive behavior, as mentioned in subsection 3.3. We remark that the dependence $I_{max} = s^{0.5}$ found in Figure 10b at the intermediate series resistance is not indicative of diffusion control.

In Figure 10c, curves of log(I_{max}) vs log(s) are plotted for the case of an exponential capacitance in parallel with an exponential charge-transfer resistance, which takes different R_{Fa} values, plus a series resistance R_s. The presence of the faradaic process causes a large departure from linear behavior. The separation is more pronounced as the faradaic current becomes more significant.

4. Discussion

The previous analysis provides an interpretation of the main features of the CVs of nanoporous TiO_2 in aqueous electrolyte reported in Figures 1−3. This interpretation is supported by the good agreement between experimental and simulated CV patterns.

From Figure 1, we may infer that the influence of faradaic processes is very small in the measured conditions (pH 2 and $s = 50$ mV s^{-1}), while in the case of Figure 3 (pH 11, $V_2 = -0.8$ V, and $s = 100$ mV), the faradaic process is the dominating effect on the CV shape. Furthermore, in this last case, with the help of impedance, we could determine that this shape, corresponding to low $\omega = sR_sC_a$, is not just due to a low faradaic resistance but also to a low capacitance, which has just activated its exponential behavior at this potential. Although not shown

here, for higher return potentials, the shape of the CV was very similar to that of Figure 1 at the highest cathodic potential.

The similarities found between experimental CVs obtained for different scan rates, Figure 2, and the simulated ones, Figure 9b, are especially relevant. Excellent agreement is found also in the representation of the dependence of I_{max} with s, Figures 5 and 10. It is now clear that most of the experimental plots of $\log(I_{max})$ vs $\log(s)$ do not follow a straight line because of the influence of charge-transfer process and that the high-speed asymptote, in which capacitance dominates over R_F, has a slope (i) smaller than one because of the series resistance and (ii) different in all of the cases because of the variation of R_s. To correct for this lack of linearity, it would be just needed to subtract the faradaic contribution to the total current at the peak V_C potential.

The understanding of major features of CVs of nanoporous semiconductors electrodes allows us now to use this fundamental electrochemical technique for a rapid assessment of the main properties of new types of electrodes and electrolytes. According to our analysis, it appears that investigating the CV response at progressively more negative return potentials and a variety of scan rates will provide sufficient information for a qualitative characterization. Looking retrospectively, we can infer by inspection that the CVs reported in the literature cover the different cases examined formerly: (i) almost purely capacitive,[15] (ii) capacitive distorted by series resistance,[13,16,18] and (iii) RC with severe parallel charge-transfer resistance.[14]

Moreover, the model described in the previous sections can be used for the quantitative analysis, and in this sense, it constitutes a tool for obtaining certain fundamental information. Therefore, a final test on the model was done by fitting the voltammogram at pH 3 of Figure 2 taken at a speed of 200 mV s^{-1} by means of an iterative process using standard software. Because the number of model parameters is large, the selection of suitable initial values is very important. To choose the best approximations, partial fits were done in the following way.

A good estimation of the value of R_s may be obtained from voltammograms taken at high values of s, when faradaic current is negligible, simply dividing the difference of potential between the point at which the current is zero and the return potential by the current at this last potential. Moreover, in these conditions of faradaic current negligible against capacitive current, the model is a simple RC circuit and a good estimation of C_a, C_b, and α may be obtained, specially when the region of low currents ($V \approx 0$) is used for the fit. In the opposite case, at low s, it is the current due to the charging of the film that can be neglected, so the model may be simplified now to the series connection of R_s and R_F, which gives the good initial values of R_{Fa}, R_{Fb}, and α_t.

Following this procedure, we were able to obtain a good fit of the experimental data, Figure 11a, which yields parameters quite similar to those given by impedance, though affected by a much greater error. From these parameters, we may estimate some physical characteristics of the nanoporous TiO_2 electrodes: (i) According to eq 13, the parameters $C_a = 3.2 \times 10^{-5}$ F cm^{-2} and $\alpha_c = 0.25$ obtained in this fit provide direct information on the charge accumulated in traps as Fermi level scans the band gap. Thus, it is possible to find accurately the charge in the TiO_2 nanoporous capacitor. Correcting the voltage scale to discount the effect of the series resistance and from elementary geometry considerations, we calculate the number of electrons per particle as a function of the film potential, V_C, presented in Figure 11b. We note that charging approaches 80 electrons per particle at the most cathodic potential. (ii) To

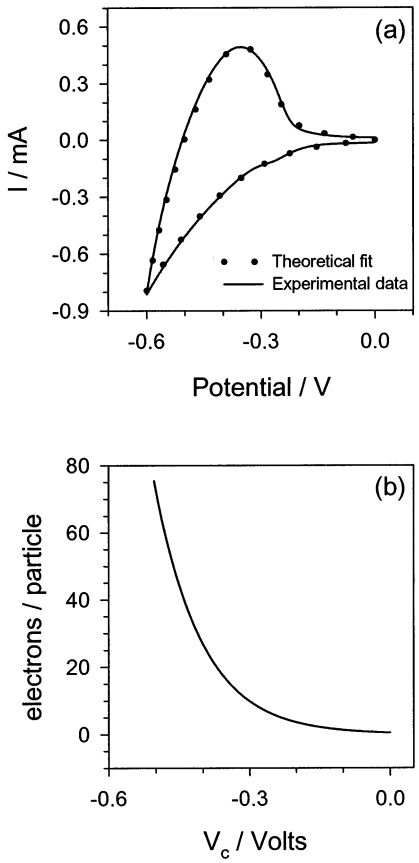

Figure 11. Theoretical fit (a), using the model discussed in the text, of a CV shown in Figure 2 for $s = 200$ mV s^{-1} and (b) electrons per particle according to the model considering an electrode surface of 2.8 cm^2, thickness of 2.6 μm, and porosity of 0.5.

completely determine the distribution of states in the energy scale, the following parameters are needed: α_c, Θ_t, and E_c. Let us denote V the working electrode potential and V_{cb} the conduction band potential with respect to the reference electrode. Using the identity $E_{cb} - E_{Fn} = e(V - V_{cb})$ and writing $C = C_a \exp[-\alpha_c eV/k_BT]$, it follows from eq 11 that

$$C_a = L \frac{\alpha_c e^2 \Theta_t}{k_B T} e^{\alpha_c eV_{cb}/(k_B T)} \tag{30}$$

We have obtained at pH 3 the parameters $C_a = 3.2 \times 10^{-5}$ F cm^{-2} and $\alpha_c = 0.25$. Equation 30 provides a link between the two remaining unknowns, Θ_t and V_{cb}. Rothenberger et al.[43] reported the potential at which nanocrystalline anatase TiO_2 particles are brought into accumulation (as measured by light absorption). According to ref 44 this potential can be identified with the conduction band potential, given by $V_{cb} = -0.40 - 0.06$ pH (V/SCE). From the value $V_{cb} = -0.58$ V vs SCE (-0.34 V vs NHE) we find $\Theta_t = 2.5 \times 10^{19}$ cm^{-3}. This calculated density is similar to that reported in ref 15. On the other hand, from the data of impedance at pH 11, we have obtained $C_a = 1.91 \times 10^{-8}$ F cm^{-2} and $\alpha_c = 0.30$. Using $V_{cb} = -1.06$ V vs SCE,[43] we obtain $\Theta_t = 2.0 \times 10^{19}$ cm^{-3}. Therefore, the resulting densities of localized states obtained by the different techniques at the two measured pHs are found consistent. The small variation may be related to the effects of band unpinning and charging of extended states, which contribute to the capacitance when $V \approx V_{cb}$, as discussed formerly, but have been neglected here for simplicity. In Figure 12, we show a schematic representation of our determination of the

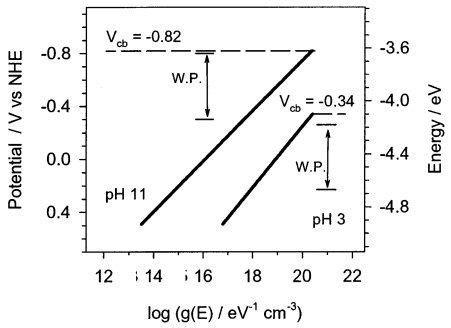

Figure 12. Schematic representation of the density of states in the band edge tail (solid line) and energy levels E_c (dashed lines) of nanocystalline TiO_2 in aqueous solution at pH 3 and 11. The ranges WP indicate the working potentials of the film at which the voltammograms and the impedance measurements have been used to determine the parameters as described in the text.

exponential distribution of localized states, indicating the region of the band gap that is scanned by the potential in each case. The density of states at the mobility edge obtained is $g(E_{cb}) = 2.4 \times 10^{20}$ cm^{-3} eV^{-1}.

5. Conclusions

Characteristic experimental voltammogram shapes have been described and simulated on the basis of a very simple model consisting of the combination of a constant resistance connected in series with the parallel combination of two exponentially potential-dependent elements: a capacitance that rises in the cathodic direction and a faradaic resistance that decreases in the same direction, as confirmed by impedance spectroscopy. The capacitance was attributed to the charging of the tail of states in the band gap, while the faradaic resistance was related with the charge losses from the film toward the electrolyte.

In a basically symmetric CV in which the current increases exponentially with voltage, it can be interpreted that the CV records directly the intrinsic film capacitance. The presence of a series resistance distorts the symmetric capacitive shape in proportion to the magnitude of current because the term R_sI takes progressively more relevance until it prevails giving a resistive regime. In these conditions, a large positive peak is observed corresponding to discharge of the charge accumulated in the capacitor while the current was negative. In the additional presence of a charge-transfer resistance, when the faradaic charge-transfer dominates, the current through the capacitor is low and the charge accumulated becomes insignificant, so the peak in positive current constitutes a minor feature or even disappears completely. When the faradaic resistance becomes very low the observed current is independent of scan direction.

As an example, a satisfactory fitting of experimental CV of nanoporous TiO_2 in aqueous electrolyte was obtained for pH 3. From these fit results, the number of electrons per particle and the distance between Fermi level and conduction band were determined. The calculated density of localized states is $\Theta_t = (2-3) \times 10^{19}$ cm^{-3}, in agreement with the calculation from impedance spectroscopy data at pH 11.

Acknowledgment. This work was supported by MCyT under Project BFM2001-3640. We thank Arie Zaban and his group for providing the samples used in this study.

Note Added after ASAP Posting. This article was released ASAP on 11/15/2002 with errors in Figure 12, eq 30, and the text discussing these data. Figure 12 was changed to take into account the correct potential of the conduction band in nanocrystalline anatase TiO_2. The previous version used the conduction band potential of rutile rather than anatase. The calculation of the density of states based on eq 30 was modified accordingly. References 43 and 44 were adjusted/added. The correct version was posted on 12/18/2002.

References and Notes

(1) Conway, B. E. *J. Electrochem. Soc.* **1991**, *138*, 1539.
(2) Pell, W. G.; Conway, B. E. *J. Power Sources* **2001**, *96*, 57.
(3) Conway, B. E.; Pell, W. G. *J. Electroanal. Chem.* **2001**, *500*, 121.
(4) Fabregat-Santiago, F.; Garcia-Belmonte, G.; Bisquert, J.; Zaban, A.; Salvador, P. *J. Phys. Chem. B* **2002**, *106*, 334.
(5) Schlichthröl, G.; Huang, S. Y.; Sprague, J.; Frank, A. J. *J. Phys. Chem. B* **1997**, *101*, 8141.
(6) Franco, G.; Gehring, J.; Peter, L. M.; Ponomarev, E. A.; Uhlendorf, I. *J. Phys. Chem. B* **1999**, *103*, 692.
(7) Bisquert, J.; Zaban, A. *Appl. Phys. A*, in press.
(8) McKinnon, W. R.; Haering, R. R. In *Modern Aspects of Electrochemistry*; White, R. E., Bockris, J. O. M., Conway, B. E., Eds.; Plenum Press: New York, 1983; Vol. 15, p 235.
(9) Chidsey, C. E. D.; Murray, R. W. *J. Phys. Chem.* **1986**, *90*, 1479.
(10) Levi, M. D.; Lopez, C.; Vieil, E.; Vorotyntsev, M. A. *Electrochim. Acta* **1997**, *42*, 757.
(11) Bisquert, J.; Zaban, A.; Salvador, P. *J. Phys. Chem. B* **2002**, *106*, 8774.
(12) Hoyer, P.; Weller, H. *J. Phys. Chem.* **1995**, *99*, 14096.
(13) Cao, F.; Oskam, G.; Searson, P. C.; Stipkala, J. M.; Heimer, T. A.; Farzad, F.; Meyer, G. J. *J. Phys. Chem.* **1995**, *99*, 11974.
(14) Lyon, L. A.; Hupp, J. T. *J. Phys. Chem.* **1995**, *99*, 15718.
(15) Boschloo, G.; Fitzmaurice, D. *J. Phys. Chem. B* **1999**, *103*, 2228.
(16) Boschloo, G.; Fitzmaurice, D. *J. Phys. Chem. B* **1999**, *103*, 7860.
(17) Lyon, L. A.; Hupp, J. T. *J. Phys. Chem. B* **1999**, *103*, 4623.
(18) Lemon, B. I.; Hupp, J. T. *J. Phys. Chem. B* **1999**, *103*, 3797.
(19) Meulenkamp, E. A. *J. Phys. Chem. B* **1999**, *103*, 7831.
(20) Redmond, G.; Fitzmaurice, D.; Grätzel, M. *J. Phys. Chem.* **1993**, *97*, 6951.
(21) Boschloo, G. K.; Goossens, A. *J. Phys. Chem.* **1996**, *100*, 19489.
(22) de Jongh, P. E.; Vanmaekelbergh, D. *J. Phys. Chem. B* **1997**, *101*, 2716.
(23) Wang, H.; He, J.; Boschloo, G.; Lindström, H.; Hagfeldt, A.; Lindquist, S. *J. Phys. Chem. B* **2001**, *105*, 2529.
(24) Fabregat-Santiago, F.; Garcia-Belmonte, G.; Bisquert, J.; Bogdanoff, P.; Zaban, A. *J. Electrochem. Soc.*, submitted for publication.
(25) Tafalla, D.; Salvador, P. *Ber. Bunsen-Ges. Phys. Chem.* **1987**, *91*, 475.
(26) Conway, B. E.; Birss, V.; Wojtowicz, J. *J. Power Sources* **1997**, *66*, 1.
(27) Peter, L. M.; Duffy, N. W.; Wang, R. L.; Wijayantha, K. G. U. *J. Electroanal. Chem.* **2002**, *524−525*, 127.
(28) Nelson, J. *Phys. Rev. B* **1999**, *59*, 15374.
(29) van de Lagemaat, J.; Frank, A. J. *J. Phys. Chem. B* **2000**, *104*, 4292.
(30) Könenkamp, R. *Phys. Rev. B* **2000**, *61*, 11057.
(31) Fisher, A. C.; Peter, L. M.; Ponomarev, E. A.; Walker, A. B.; Wijayantha, K. G. U. *J. Phys. Chem. B* **2000**, *104*, 949.
(32) Zaban, A.; Meier, A.; Gregg, B. A. *J. Phys. Chem. B* **1997**, *101*, 7985.
(33) Bisquert, J.; Garcia-Belmonte, G.; Fabregat-Santiago, F. *J. Solid State Electrochem.* **1999**, *3*, 337.
(34) Böttger, H.; Bryksin, V. V. *Hopping Conduction in Solids*; Akademie Verlag: Berlin, 1985.
(35) Tyagi, M. S. *Introduction to Semiconductor Materials and Devices*; John Wiley and Sons: New York, 1991.
(36) Bisquert, J. *Electrochim. Acta* **2002**, *47*, 2435.
(37) Bisquert, J.; Vikhrenko, V. S. *Electrochim. Acta* **2002**, *47*, 3977.
(38) Knebel, O.; Lauermann, I.; Pohl, J. P.; Uhledorf, I. *12th Int. Conf. Photochem. Convers. Storage Sol. Energy, Berlin (Ger.)* **1998**, Abstract 1W34.
(39) Hoai, T. X.; Tinh, N. T.; Duc, T. T. *14th Int. Conf. Photochem. Convers. Storage Sol. Energy, Saporo (Jpn.)* **2002**, Abstract W6-O-6.
(40) Boschloo, G.; Fitzmaurice, D. *J. Phys. Chem. B* **1999**, *103*, 3093.
(41) zum Felde, U.; Haase, M.; Weller, H. *J. Phys. Chem. B* **2000**, *104*, 9388.
(42) Peter, L. M.; Riley, D. J.; Wielgosz, R. I. *Appl. Phys. Lett.* **1995**, *66*, 2355.
(43) Rothenberger, G.; Fitzmaurice, D.; Grätzel, M. *J. Phys. Chem.* **1992**, *96*, 5983.
(44) Hagfeldt, A.; Grätzel, M. *Chem. Rev.* **1995**, *95*, 49.